Underestimated permafrost landforms – Block and talus slope distribution in the Dry Andes of Argentina

Tamara Köhler[1], Anna Schoch-Baumann[1], Rainer Bell[1], Diana Agostina Ortiz[1], Philipp Reichartz[1], Lothar Schrott[1] & Dario Trombotto Liaudat[2]

[1]*Department of Geography, University of Bonn, Meckenheimer Allee 166, 53115 Bonn, Germany*

[2]*Geocryology, IANIGLA, CCT CONICET Mendoza, Argentina*

ABSTRACT

There is a lack of explanatory approaches and analytical data on distribution patterns, landform characteristics and formative controls of block and talus slopes in the Dry Andes of Argentina, despite these being widespread and characteristic elements of the extensive periglacial belt. Their spatial distribution, internal structure and ice content have received far less attention than rock glaciers, which are included in regional and national inventories and have been studied systematically in the last decades (e.g., IANIGLA-CONICET, 2018). We extend these inventories by block and talus slopes based on a remote-sensing and field-based geomorphological mapping approach in the Agua Negra catchment (30°S, 69°W). Three sub-catchments were chosen for the manual mapping approach, reflecting the overall heterogeneity of the study area and ensuring transferability. Analysis of the uppermost sub-catchment alone reveals that only 1.6% of the surface are covered by rock glaciers, while block and talus slopes cover almost 80%. These landforms are by far the most dominant geomorphic features in the basin, typical in this part of the Andes and probably—in terms of surface area, vertical extension and permafrost distribution—unique in mountain systems worldwide. By using geomorphological mapping and statistical evaluation, spatial distribution patterns are captured and analyzed, thus providing the foundation for further analyses such as geophysical prospection and upscaling. Especially in light of global climate change, understanding the spatial distribution of potentially ice-rich permafrost landforms is imperative to assess available water resources, water quality and their evolution.

1 INTRODUCTION

The Andean cryosphere is an important hydrological reservoir that controls runoff and groundwater recharge through glacier melt, precipitation, snowmelt, and water releases from the active layer in permafrost areas (Masiokas et al. 2020; Halla et al. 2021). Especially in drought-prone areas with limited glaciation, periglacial landforms are hydrologically significant (Schaffer et al. 2019; Masiokas et al. 2020). Their delayed response to global warming will even increase their importance in the future (Schaffer et al. 2019; Arenson et al. 2022). The observed rapid glacier retreat, the significant decrease in snowfall and snow persistence as well as the increased permafrost degradation in the Argentinian Andes due to global climate change were addressed in 2010 with a national statute to protect glaciers and the periglacial environment (Masiokas et al. 2020; Blöthe et al. 2021). One of the most important outcomes was the creation of a national glacier inventory, mapping cryospheric landforms under protection (IANIGLA-CONICET 2018).

Within the Dry Andean periglacial belt, the most visible expression of mountain permafrost are rock glaciers, whose distribution and internal structure have been studied systematically (Villarroel et al. 2018; Blöthe et al. 2021; Halla et al. 2021). They are recorded in the Argentinian national inventory, while more widespread permafrost-affected block and talus slopes have received less attention. Talus slopes are sheeted and cone-shaped debris accumulations below free rock faces mainly fed by rockfall (Lambiel and Pieracci 2008; Kenner et al. 2017). They are characteristic features of periglacial mountain regions and have been subject to frequent research (e.g., Sass 2006; Lambiel and Pieracci 2008; Scapozza et al. 2015; Kenner et al. 2017). Studies on periglacial talus slopes in the Swiss Alps found possible ice contents of about 20–60% (Scapozza et al. 2015). However, there is a significant data gap in the Andes, where they were mainly examined as debris sources of talus-derived rock glaciers (e.g., Halla et al. 2021), or in terms of debris movement (Pérez 1993) and hydrological characteristics (Caballero et al. 2002). Even less research on a global scale has been devoted to blockslopes, which is not least due to varying terminology and definitions. Blockslopes, often also termed rectilinear debris-mantled slopes (Kamp et al. 2005; Trombotto Liaudat et al. 2014; French 2017) or Richter (denudation) slopes (Augustinus and Selby 1990; Fort and van Vliet-Lanoe 2007) are straight slopes of in situ weathered material. They were mainly described in the ice-free areas of Antarctica (e.g., Augustinus and Selby 1990; French 2017). Earlier studies mention their vast distribution in the semiarid to arid Andes (Garleff and Stingl 1983; Trombotto 2000; Kamp et al. 2005). If these landforms contain a not yet quantified amount of ice, they gain hydrological significance due to their large distribution in the Andes. Thus, our study investigates the spatial distribution of taluses and blockslopes in a semiarid high Andean catchment by combining geomorphological mapping and statistical terrain analysis. Our results are an extension of the existing national inventory on cryospheric landforms (IANIGLA-CONICET 2018), to quantify these underestimated permafrost landforms in the Dry Andes of Argentina.

https://doi.org/10.52381/ICOP2024.151.1

2 Study Area

The Agua Negra catchment (ANC) is located in the Cordillera Frontal of the San Juan province in the Dry Andes of Argentina. It is part of the Desert Andes near the southern transition to the Central Andes (Esper Angillieri 2009), where we can see a distinct increase in cryospheric landform cover reaching down to about 3000 m asl (Figure 1). The Desert Andes are characterized by extremely low mean annual precipitation (< 250 mm) mainly falling during winter months as snow or sleet above 4000 m asl (Minetti et al. 1986; Lliboutry 1998). Snow cover is comparatively thin and of short duration (~3 months) due to the effect of high incoming solar radiation throughout the year, controlling surface temperatures and upper ground thermal regimes (Schrott 1994; Lliboutry 1998). The drier conditions in this part of the Dry Andes are also reflected by the distribution of cryogenic landforms in terms of areal coverage and altitude (Figure 1c). The median 0 °C isotherm rises by almost 1000 m compared to the Central Andes, as does the lower limit of glaciers. Rock glacier distribution is mainly concentrated in an altitudinal band between 4500 and 5000 m asl. While the areal extent of glaciers clearly dominates over periglacial forms in the Central Andes, the importance of the latter increases significantly in the Desert Andes (Sattler et al. 2016). Information on the geology is only available in coarse resolution and indicates that the ANC comprises different geological units. The Paleozoic basement of marine sedimentary rocks and local granite intrusions is covered mainly by Permian to Triassic volcanic and volcanoclastic rocks of the Choiyoi Group, accounting for almost 64% of the upland area (SEGEMAR 2019).

Within an area of 1315 km^2 the ANC covers an altitudinal range of 4735 m, with the highest peak reaching 6280 m asl. The mean precipitation dataset of the Climate Hazards Group InfraRed Precipitation with Station data (CHIRPS) from 1981 to 2020 (Funk et al. 2014) shows a mean precipitation sum of about 53 mm/yr in the lowland parts of the catchment and up to 131 mm/yr in the upland. A meteorological station in front of the Agua Negra glacier reports high global radiation values of ~430 W/m^{2}d^{-1} and low mean relative humidity of ~30% (Pitte et al. 2022). Scattered morainic remnants detectable in the whole ANC as well as the U-shaped main valley prove the more extensive glacial imprint in the catchment in the past. However, no mapping of moraines or stratigraphical studies indicating Pleistocene glaciations are available for this part of the Andes. At present, the basin shows regionally representative cryospheric conditions (Gruber 2012; IANIGLA-CONICET 2018), enabling the transferability of the results within the semiarid Argentinean Andes. It has a low glacial coverage of 1.44% and a large vertical extent of mountain permafrost of almost 2600 m with respect to the regional lower permafrost limit at ~3700 m asl (Trombotto 2000; Gruber 2012). In the entire catchment, 59 rock glaciers are mapped (IANIGLA-CONICET 2018), comprising an area of 5 km^2 or 0.38%. With 667.78 km^2 identified as areas with potential permafrost (Gruber 2012; Figure 1b) there is a clear spatial deviation between the mapped rock glaciers and the potential permafrost distribution.

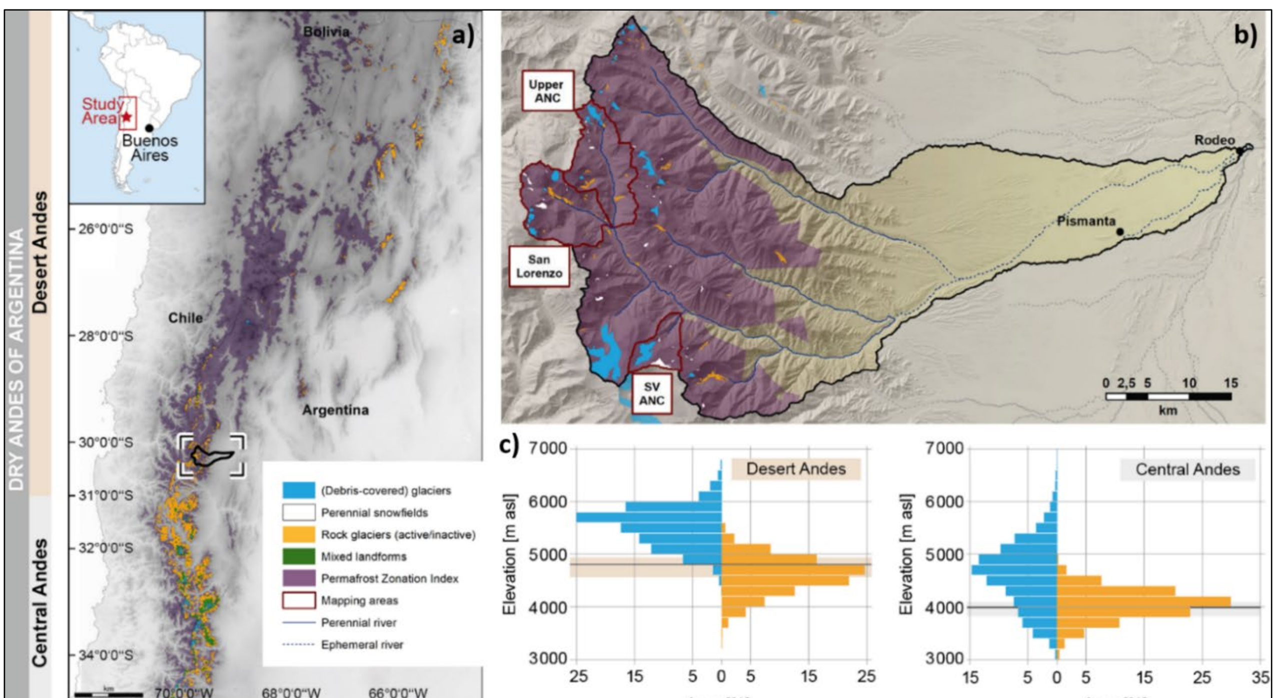

Figure 1. a) Overview of the location and cryospheric composition of the Dry Andes of Argentina, with c) the regional area-elevation distribution of glacial and periglacial landforms including the median elevation of the 0 °C isotherm surrounded by 25–75 % quantiles, calculated from ERA-5 monthly re-analysis data averaged from 1940 to present (Hersbach et al. 2023). b) Detailed overview of the study area of the Agua Negra catchment with the manual mapping areas. Permafrost Zonation Index (very low to high possibilities) based on Gruber (2012), cryospheric landforms taken from IANIGLA-CONICET (2018). Landforms in a) were optically enlarged by a 1-pt frame to enable visibility.

The basin is drained by the Agua Negra River and its tributaries, mainly fed by the meltwaters of surrounding glaciers and seasonal to perennial snowfields, precipitation, as well as contributions from active layer thawing and permafrost degradation (Halla et al. 2021, Schrott 1996). Discharge measurements confirmed that water released from the active layer and seasonally frozen ground may constitute ~30% of total discharge during the summer months in the upper ANC (Schrott 1996).

3 Methods

We conduct a remote sensing and field-based geomorphological mapping approach of block and talus slopes in three sub-catchments of the ANC, building on the existing national inventory of cryospheric landforms (IANIGLA-CONICET 2018; Figure 1). Our mapping results are statistically evaluated to analyze the spatial distribution, characteristics and formative controls of the target landforms.

3.1 Geomorphological mapping

A geomorphological map of blockslopes, taluses and bedrock was created based on satellite imagery (Esri, Google Earth Pro) and a TanDEM-X DEM (12 m resolution). We used satellite imagery from austral summer months with minimum snow cover and shading to improve mapping accuracy. The upper ANC, San Lorenzo catchment (SLC) and a side valley in the ANC (SV ANC) were selected for manual mapping to reflect the overall heterogeneity of the basin. All three sub-catchments lie within the Permafrost Zonation Index (Gruber 2012, Figure 1a, b). Furthermore, their altitudinal range, valley orientation, size and ratio of glacial and periglacial landforms is representative. Rock glaciers, (debris-covered) glaciers and perennial snowfields (IANIGLA-CONICET 2018) as well as bedrock (manually mapped) were used to support mapping accuracy and to allow for a comparative spatial quantification of all cryospheric landforms in the sub-catchments. The inventory-based, restricted rock glacier delineation was extended to include front and marginal parts (RGIK 2022). The final output is an extended geomorphological map of cryospheric landforms (Figure 2), accurately delineating blockslopes and taluses that serve as input for the statistical analysis.

3.2 Statistical Analysis

A pixel-based analysis of block and talus slope distribution based on 15 individual variables reflecting topography, surface morphology and climatic conditions on different spatial scales was conducted to determine their spatial distribution, landform characteristics and formative controls (Table 1). In addition, the statistical analysis provides valuable insights into the suitability of the applied variables for future geostatistical modeling and semi-automatic mapping of block and talus slopes on a larger spatial scale. Since there is little information on suitable variables characterizing the distribution of blockslopes and taluses, we selected and adopted variables from comparable landform distribution studies in (periglacial) mountain landscapes (see references in Table 1). The original and

Table 1. Input variables for the statistical analysis calculated on different resolutions (12 m original TanDEM-X; *60 m resampled TanDEM-X using bilinear interpolation). ([1]Blöthe et al. 2021; [2]Brenning 2009; [3]Deluigi et al. 2017; [4]Groh and Blöthe 2019; [5]Heckmann et al. 2014; [6]IANIGLA-CONICET 2018; [7]Janke 2013; [8]Cavalli et al. 2013; [9]Otto et al. 2018; [10]Riley et al. 1999; [11]Sattler et al. 2016; [12]Schoch et al. 2018; [13]Weiss 2001).

Variable	Description	References (sel.)
Elevation	Altitude [m asl]	[3] [4]
Slope	Slope gradient [°]	[5] [11] [12]
Topographic position index (TPI_{33})	Topographic slope position based on elevation comparison of one cell to its surrounding neighborhood in a rectangular 33x33 cell moving window $TPI = z_0 - z_{mean}$ [1]	[13]
Curvature* (overall, planform, profile)	*Overall, planform (vertical) and profile (horizontal)* slope concavity and convexity	[3] [4] [5] [7]
Aspect	*North-exposedness*, cosine of the aspect	[1] [3] [12]
	East-exposedness, sine of the aspect	[1] [12]
Potential incoming solar radiation (PISR)	For the entire year 2022 based on topographic position and relief (DEM) [MWh/m^2]	[3] [11]
Topographic wetness index (TWI)	Areas with topography-controlled water accumulation defined by slope (ß) and upstream contributing area based on the D8-flow algorithm (A) $TWI = \ln(A / \tan(ß))$ [2]	[9]
Topographic roughness index (TRI, TRI_{60}*)	Elevation difference from a center cell and its surrounding neighborhood in a 3x3 cell moving window	[5] [9] [10]
Size of the contributing area (SCA)	Size of the contributing area [m^2], calculated using the D8-flow algorithm, log-transformed	[2] [4] [12]
Mean roughness of the contributing area (MRCA)	TRI-weighted flow accumulation divided by unweighted flow accumulation (D8-flow algorithm)	[5] [8]
Mean slope of the contributing area (MSCA)	Slope-weighted flow accumulation divided by unweighted flow accumulation (D8-flow algorithm)	[2] [4] [12]

the resampled (60 m) TanDEM-X DEM were used to analyze differences in the distribution and landform characteristics on several spatial scales.

We applied parameters representing topographic conditions and surface morphology (e.g., curvature, topographic roughness) as well as landform characteristics (e.g., slope inclination, different characteristics of the contributing area). To represent climatic and moisture conditions, the elevation as well as the potential incoming solar radiation (PISR) and topographic wetness (TWI) were used, since there is no meteorological network to interpolate climatic variables from measured data. The coarse resolution of satellite-derived meteorological data is insufficient for the study purpose and highly uncertain in high mountains.

Boxplots are used to summarize, examine and compare the distribution of the target landforms visually for each variable. Differences in the distribution of explanatory variables for block and talus slopes were tested for significant statistical differences ($p < 0.05$) using the Kruskal-Wallis and the Wilcoxon rank sum test for non-parametric data. Here, we present a summary of the combined analysis, detailed results of the single sub-catchments can be accessed online (http://dx.doi.org/10.13140/RG.2.2.24348.67200/1).

4 Results

Block and talus slopes are widely distributed in all three sub-catchments (Figure 2). Blockslopes are by far the most dominant landform accounting for more than 60% of the areal surface. In the Upper ANC and SLC, talus slopes are the secondary landform with ~12% areal coverage, while in the more glacier and snow influenced SV ANC they account for only 2.4%. In the upper ANC, a distinct difference between the main valley slopes bordering the Agua Negra River can be observed. West of the small mountain stream with dominant slope exposures to N and E, blockslopes have a vast and uniform distribution. On the eastern valley slopes, the proportion of extensive talus sheets and coalescing talus cones below (channelized) steep cliffs increases. More than 60% of the talus coverage in the Upper ANC is located east of the Agua Negra River. The dominance of blockslopes on N and E exposed slopes is also very evident in the SV ANC, as well as southwest of the San Lorenzo stream in the SLC, though less distinct. Both landforms exhibit statistically significant ($p < 0.05$) differences for all analyzed variables, enabling statements about the distribution and formation conditions (Figure 3). As represented by the topographic position index (TPI), blockslopes mainly cover low relief plateaus and upper to middle slopes, sparsely dissected by alluvial channels or bedrock outcrops. Talus slopes primarily occur in lower slope positions bordering channels and river floodplains. The elevation differences of the landforms are particularly notable (Figure 3). Even though blockslopes were mapped at nearly all considered elevations, they are dominating between 4900 m and 5500 m asl, with an elevation mean at 5194 m asl. Talus slopes, however, are distributed in a narrower interquartile range of 4300 m and 4700 m asl with a mean elevation of 4540 m asl and an upper limit of ~5300 m asl. Upslope they are limited by bedrock outcrops feeding the talus that are incorporated in the statistical analysis due to their higher roughness values. Hence, the mean roughness values of the contributing area (MRCA) are higher. Large bedrock outcrops on the middle and upper slopes are also associated with thick talus formation. Where the material is additionally channelized, cone-

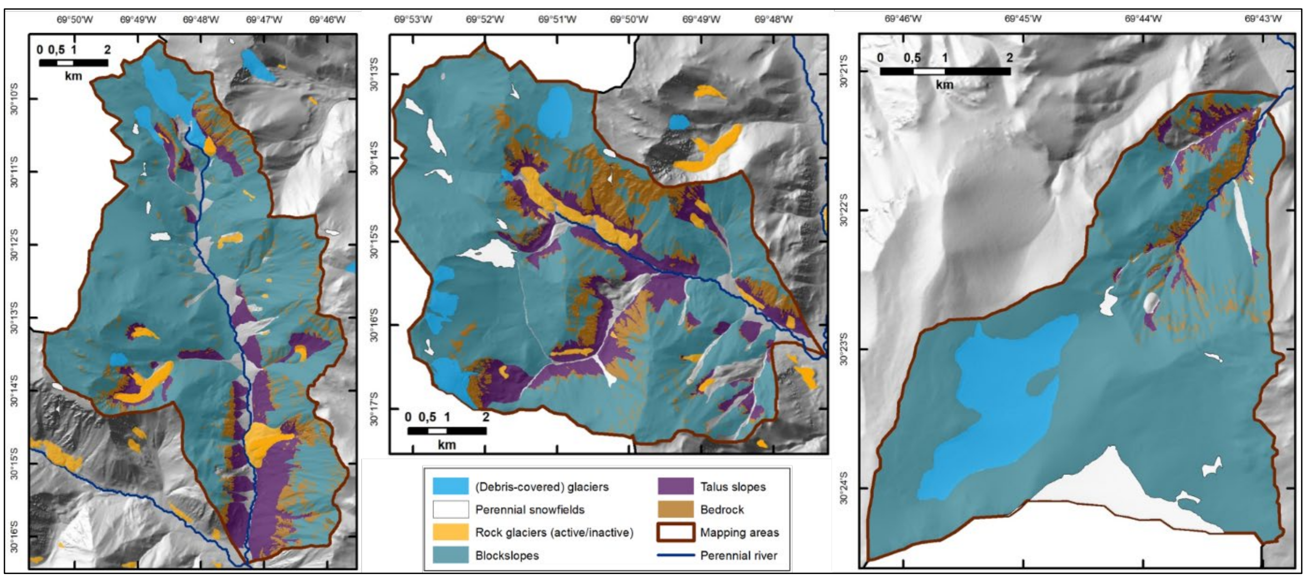

Figure 2. Geomorphological maps of blockslope, talus and bedrock distribution in the three sub-catchments of the Agua Negra catchment, with (from left to right) the Upper Agua Negra catchment (Upper ANC), San Lorenzo catchment (SLC) and the side valley farther downstream the Agua Nera catchment (SV ANC); see Figure 1 for locations. (Debris-covered) glaciers, perennial snowfields and rock glaciers from IANIGLA-CONICET (2018). The map shows the extended rock glacier outline including frontal and marginal parts (based on RGIK 2022). Note the different scales of the catchments.

shaped taluses, protalus ramparts and talus-derived rock glaciers can be found.

Talus slopes are characterized by greater mean slope inclination around 25–28° of the landform itself, but also of the contributing area (MSCA). Blockslopes mainly range from 17–22°. Despite their different slope angles, both slope types mainly occur horizontally and vertically elongate, although this pattern is much more distinct for blockslopes. For blockslopes, all three curvature layers show mean values of ±0.0, indicating a remarkable slope linearity in horizontal and vertical direction. Talus slopes, however, display a tendency towards horizontal and vertical concavity, indicated by slightly positive profile and slightly negative planform curvature (Figure 3).

While talus slopes show no clear tie to aspect except for a certain dominance in southern exposures in the three sub-catchments, blockslopes occur more frequently on N and E-facing hillsides, resulting in higher insolation (+ 0.34 MWh m^{-2}). The topographic roughness indices TRI and TRI_{60} indicate higher roughness for taluses with the latter one showing more pronounced differences between the two landforms. Although the distributional differences between blockslopes and taluses are statistically significant for all examined variables, the TWI shows the smallest effect on their distribution patterns. Both landforms show the same tendency towards low potential topographic water accumulation, and differences in contributing area sizes (SCA) are rather small. Taluses have slightly larger catchments on average, corresponding to their topographic positions in the catchments.

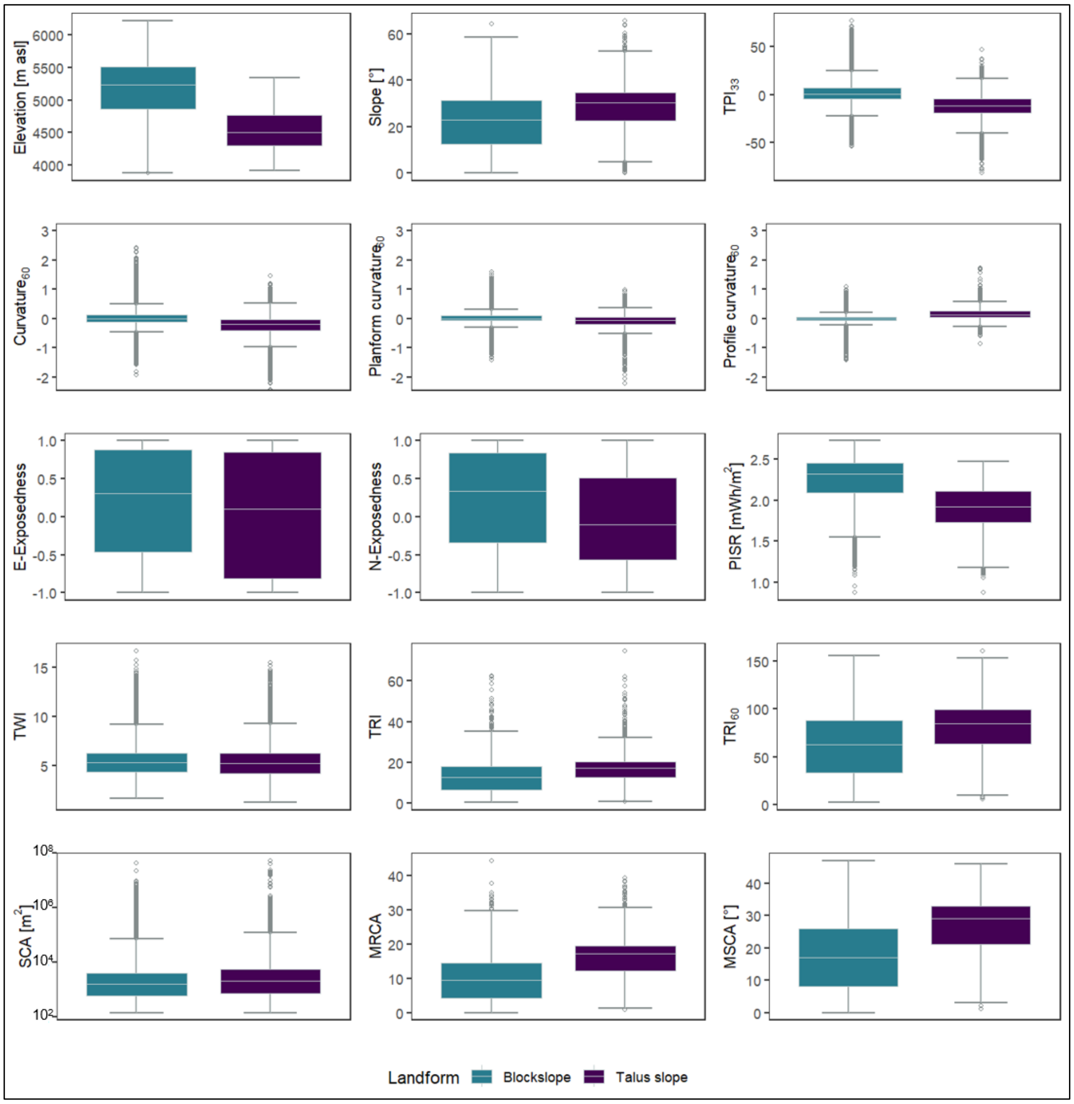

Figure 3. Boxplots showing the median and interquartile range for the analyzed environmental variables for both target landforms in all three manual mapping areas (further details and abbreviations in Table 1). Block and talus slopes show statistically significant differences ($p < 0.05$) for all examined variables.

4 DISCUSSION

The statistical analysis of the environmental characteristics of block and talus slopes point out important factors for their formation. The distribution of variables allows inferences about the characteristics and distribution of the landforms. The exceptionally high insolation associated with the semiarid, leeward climatic conditions in the Dry Andes of Argentina seem to greatly favor blockslope formation. Their apparent distribution on high elevation, low-relief plateaus and sparsely dissected, preferentially N and E-exposed upper slopes imply suitable conditions there. Thus, the development of blockslopes seems to be linked to these cold and (semi)arid conditions (e.g., Trombotto Liaudat et al. 2014; French 2017). Their wide distribution at high altitudes, mainly above 5000 m asl, in combination with high exposure to incoming solar radiation benefits strong temperature gradients, effective frost action as well as evaporation and sublimation. This is confirmed by Höllermann (1983), who describes their most common distribution in the upper part of the periglacial or subnival belt at 30–50°N and 29–35°S, with their greatest vertical extent at 30°N and 30°S in sunny exposures. Further variables like a wind shelter index (Veitinger et al. 2016) or geomorphic protection index (Kofler et al. 2020) might be useful for interpretation, as strong wind action in topographically open areas is supposed to contribute to blockslope formation via debris-removal, wind-drift, enhancing dryness and in situ weathering (Garleff and Stingl 1983; Höllermann 1983). The connection of blockslope formation to dry conditions is further supported by very low TWI values. However, talus slopes feature nearly the same TWI values. This is inconsistent with other variables, e.g., curvature, PISR, TPI and N-exposedness that indicate talus occurrence on lower slope positions with higher water-converging planform and profile curvature, and lower insolation (cf. Etzelmüller et al. 2006). The slight upward concavity and intersecting channels observed for talus slopes favor the concentration of water flow and snow accumulation through wind sheltering, thus suggesting higher water availability. A stronger topographic shading matching the smaller PISR can be derived from their higher occurrence on south-facing, lower slope positions in rugged, intersected terrain. Associated protalus rampart and talus-derived rock glacier formation is a clear indication for a certain water availability and moisture content.

We assume that debris supply from the bedrock cliffs exceeds the material removal mainly occurring at the lower talus, since the investigated taluses have a straight to slightly concave profile curvature and a decreasing slope inclination between rock wall and talus (cf. Sass 2006). Thus, sediment storages of considerable size can build up (Otto 2006). The higher slope inclinations of taluses and associated contributing areas indicate a higher angle of repose for talus accumulations beneath steep feeder rock walls compared to blockslopes. This is in accordance with our field observations of coarse-grained talus material compared to finer-grained blockslopes (cf. Otto, 2006). A higher resolution DEM is necessary to visualize grain size differences between blockslopes and taluses with the TRI. The overall higher TRI and TRI_{60} on taluses result from the smaller landform extent in combination with their topographic position bordering large bedrock outcrops, floodplains, incised channels, protalus ramparts and rock glaciers. Due to the coarse resolution of the roughness indices, these are included in the analyses and produce higher values that are not necessarily linked to landform characteristics or formation controls, but distributional patterns. The high range of roughness indices for blockslopes is largely driven by isolated bedrock outcrops below the lower mapping limit of bedrock (30 m^2), which are thus included in the blockslope analysis. Apart from these, blockslopes feature neither evident source areas, nor indications for dominant erosion and deposition with respect to curvature, roughness and slope inclination. Therefore, the presence of a rather thin layer of debris above in situ weathered bedrock is plausible and supported by Trombotto (1991), reporting only thin cryoregolith deposits. The thin debris layer migrates downslope by gravitational processes like (perma)frost creep (Fort and van Vliet-Lanoe 2007; Trombotto Liaudat et al. 2014). Debris supply and debris removal seem to be largely in equilibrium, resulting in the characteristic slope shape at repose angles of the underlying bedrock (French 2017). Their characteristic straight shape without significant channelization or de-/acceleration of debris is reflected in the name "rectilinear" slopes (Trombotto Liaudat et al. 2014; French 2017).

Based on the insulating effect of the thick debris layer and the above-mentioned topographically favorable conditions, we expect higher permafrost probabilities and ice contents in talus slopes than in blockslopes (Lambiel and Pieracci 2008). Trombotto (1991) found not only seasonal ice but permafrost in the taluses of Lagunita del Plata in the Central Andes (33°S, 69°W). In the Swiss Alps, the presence of ice-rich permafrost was mainly reported in the lower parts of the talus slopes with the greatest sediment thickness (Lambiel and Pieracci 2008; Scapozza et al. 2015). Ground ice volumes are presumably lower in blockslopes due to the extremely low TWI, high exposure to insolation and wind as well as a rather thin insulating debris layer with minor impact on ground ice protection. In addition, the low sediment thickness offers smaller storage capacities compared to thick talus accumulations. Nevertheless, the blockslope occurrence in cold and (semi)arid environments provides suitable conditions for permafrost formation (see also Permafrost Zonation Index, Figure 1) and they have been reported in areas with continuous permafrost around this latitude (e.g., Trombotto 2000; Kamp et al. 2005). The potentially low ice contents must be considered in context with their large distribution to make accurate quantifications on different spatial scales.

5 CONCLUSIONS AND OUTLOOK

Block and talus slopes are dominant in the periglacial belt of the Dry Argentinian Andes, accounting for 77.5% (67% blockslopes, 10.5% talus slopes) of the mapped sub-catchments in the ANC. Rock glaciers, by contrast, cover only 1.5% (IANIGLA-CONICET 2018). We demonstrate that both landforms provide suitable permafrost conditions for the presence of ground ice and may gain hydrological significance due to their large extent compared to other periglacial landforms. Talus slopes feature more favourable conditions for permafrost formation and conservation due to higher insulation capacity of thick debris accumulations in sheltered, water converging lower slope positions. Blockslopes are exposed to higher insolation and frost action at high altitudes in topographically open upper slope positions and plateaus, forming a small layer of in situ weathered debris with potentially lower ice contents. To further assess their role as runoff contributors in the Dry Andes of Argentina, we need distribution analyzes at larger spatial scales and the investigation of their internal structure and potential ice content. These studies gain additional importance in the context of global warming and the depletion of glacial water resources.

6. References

Arenson, L.U., Harrington, J.S., Koenig, C.E.M., and Wainstein, P.A. 2022. 'Mountain Permafrost Hydrology—A Practical Review Following Studies from the Andes', *Geosciences* 12(2), p. 48.

Augustinus, P.C. and Selby, M.J. 1990. 'Rock Slope Development in Mcmurdo Oasis, Antarctica, and Implications for Interpretations of Glacial History', *Geografiska Annaler: Series A, Physical Geography* 72(1), pp. 55–62.

Blöthe, J.H., Halla, C., Schwalbe, E., Bottegal, E., Trombotto Liaudat, D., and Schrott, L. 2021. 'Surface velocity fields of active rock glaciers and ice-debris complexes in the Central Andes of Argentina', *Earth Surface Processes and Landforms* 46(2), pp. 504–522.

Brenning, A. 2009. 'Benchmarking classifiers to optimally integrate terrain analysis and multispectral remote sensing in automatic rock glacier detection', *Remote Sensing of Environment* 113(1), pp. 239–247.

Caballero, Y., Jomelli, V., Chevallier, P., and Ribstein, P. 2002. 'Hydrological characteristics of slope deposits in high tropical mountains (Cordillera Real, Bolivia)', *CATENA* 47(2), pp. 101–116.

Cavalli, M., Trevisani, S., Comiti, F., and Marchi, L. 2013. 'Geomorphometric assessment of spatial sediment connectivity in small Alpine catchments', *Geomorphology*, pp. 31–41.

Deluigi, N., Lambiel, C., and Kanevski, M. 2017. 'Data-driven mapping of the potential mountain permafrost distribution', *The Science of the total environment* 590–591, pp. 370–380.

Esper Angillieri, M.Y. 2009. 'A preliminary inventory of rock glaciers at 30°S latitude, Cordillera Frontal of San Juan, Argentina', *Quaternary International* 195(1–2), pp. 151–157.

Etzelmüller, B., Heggem, E.S.F., Sharkhuu, N., Frauenfelder, R., Kääb, A., and Goulden, C. 2006. 'Mountain permafrost distribution modelling using a multi-criteria approach in the Hövsgöl area, northern Mongolia', *Permafrost and Periglacial Processes* 17(2), pp. 91–104.

Fort, M. and van Vliet-Lanoe, B. 2007. 'Permafrost and periglacial environment of Western Tibet', *Landform Analysis* 5, pp. 25–29.

French, H.M. 2017. *The periglacial environment*. Hoboken, NJ, USA: John Wiley & Sons.

Funk, C.C., Peterson, P.J., Landsfeld, M.F., Pedreros, D.H., Verdin, J.P., Rowland, J.D., Romero, B.E., Husak, G.J., Michaelsen, J.C., and Verdin, A.P. 2014. 'A quasi-global precipitation time series for drought monitoring', *US Geological Survey Data Series* 832. doi: https://doi.org/10.3133/ds832.

Garleff, K. and Stingl, H. 1983. 'Hangformen und Hangformung in der periglazialen Höhenstufe der argentinischen Anden zwischen 27° und 55° südliche Breite' in Poser and Schunke (eds.) *Mesoformen des Reliefs im heutigen Periglazialraum. Abhandlungen der Akademie der Wissenschaften Göttingen* 3(35), pp. 425–434.

Groh, T. and Blöthe, J.H. 2019. 'Rock Glacier Kinematics in the Kaunertal, Ötztal Alps, Austria', *Geosciences* 9(9), p. 373.

Gruber, S. 2012. 'Derivation and analysis of a high-resolution estimate of global permafrost zonation', *The Cryosphere* 6(1), pp. 221–233.

Halla, C., Blöthe, J.H., Tapia Baldis, C., Trombotto Liaudat, D., Hilbich, C., Hauck, C., and Schrott, L. 2021. 'Ice content and interannual water storage changes of an active rock glacier in the dry Andes of Argentina', *The Cryosphere* 15(2), pp. 1187–1213.

Heckmann, T., Gegg, K., Gegg, A., and Becht, M. 2014. 'Sample size matters: investigating the effect of sample size on a logistic regression susceptibility model for debris flows', *Natural Hazards and Earth System Sciences* 14(2), pp. 259–278.

Hersbach, H., Bell, B., Berrisford, P., Biavati, G., Horányi, A., Muñoz Sabater, J., Nicolas, J., Peubey, C., Radu, R., Rozum, I., Schepers, D., Simmons, A., Soci, C., Dee, D., and Thépaut, J.-N. (2023). 'ERA5 monthly averaged data on pressure levels from 1940 to present', *Copernicus Climate Change Service (C3S) Climate Data Store (CDS)*. Available at: https://cds.climate.copernicus.eu/cdsapp#!/dataset/reanalysis-era5-pressure-levels-monthly-means?tab=overview.

Höllermann, P. 1983. 'Verbreitung und Typisierung von Glatthängen', in Poser and Schunke (eds.) *Mesoformen des Reliefs im heutigen Periglazialraum. Abhandlungen der Akademie der Wissenschaften Göttingen* 3(35), pp. 241–260.

IANIGLA-CONICET, Ministerio de Ambiente y Desarrollo Sustentable de la Nación 2018. 'IANIGLA-Inventario Nacional de Glaciares', *Informe de la subcuenca del río Blanco*. Cuenca del río San Juan, p. 62.

Janke, J.R. 2013. 'Using airborne LiDAR and USGS DEM data for assessing rock glaciers and glaciers', *Geomorphology* 195, pp. 118–130.

Kamp, U., Bolch, T., and Olsenholler, J. 2005. 'Geomorphometry of Cerro Sillajhuay (Andes, Chile/Bolivia): Comparison of Digital Elevation Models (DEMs) from ASTER Remote Sensing Data and Contour Maps', *Geocarto International* 20(1), pp. 23–33.

Kenner, R., Phillips, M., Hauck, C. Hilbich, C., Mulsow, C., Bühler, Y., Stoffel, A., and Buchroithner, M. 2017. 'New insights on permafrost genesis and conservation in talus slopes based on observations at Flüelapass, Eastern Switzerland', *Geomorphology* 290, pp. 101–113.

Kofler, C., Steger, S., Mair, V., Zebisch, M., Comiti, F., and Schneiderbauer, S. 2020. 'An inventory-driven rock glacier status model (intact vs. relict) for South Tyrol, Eastern Italian Alps', *Geomorphology* 350, 106887.

Lambiel, C. and Pieracci, K. 2008. 'Permafrost distribution in talus slopes located within the alpine periglacial belt, Swiss Alps', *Permafrost and Periglacial Processes* 19(3), pp. 293–304.

Lliboutry, L. 1998. 'Glaciers of the Dry Andes (Glaciers of Chile and Argentina' in R.S. Williams Jr. and J.G. Ferrigno (eds.) *Satellite image atlas of glaciers of the world South America* U.S. Geological Survey Professional Paper 1386-I, pp. 1109–1147.

Masiokas, M.H., Rabatel, A., Rivera, A., Ruiz, L., Pitte, P., Ceballos, J.L., Barcaza, G., Soruco, A., Bown, F., Berthier, E., Dussaillant, I., and MacDonell, S. 2020. 'A Review of the Current State and Recent Changes of the Andean Cryosphere', *Frontiers in Earth Science* 8, p. 99.

Minetti, J.L., Barbieri, P.M., Carletto, M.C., Poblete, A.G., and Sierra, E.M. 1986. 'El régimen de precipitatiòn de la provincia de San Juan', *Informe técnico 8*. CIRSAJ-CONICET, San Juan.

Otto, J.-C. 2006. *Paraglacial sediment storage quantification in the Turtmann Valley, Swiss Alps*. Doctoral dissertation at the University of Bonn, Germany.

Otto, J.-C., Prasicek, G., Blöthe, J., and Schrott, L. 2018. 'GIS applications in geomorphology' in B. Huang (ed.) *Comprehensive Geographic Information Systems*. Bonn, GER: Elsevier Inc., pp. 81–111.

Pérez, F.L. 1993. 'Talus movement in the high equatorial Andes: A synthesis of ten years of data', *Permafrost and Periglacial Processes* 4(3), pp. 199–215.

Pitte, P., Masiokas, M., Gargantini, H., Ruiz, L., Berthier, E., Ferri Hidalgo, L., Zalazar, L, Dussaillant, I., Viale, M., Zorzut, V., Corvalán, E., Scarpa, J.P., Costa, G., and Villalba, R. 2022. 'Recent mass-balance changes of Agua Negra glacier (30°S) in the Desert Andes of Argentina', *Journal of Glaciology* 68(272), pp. 1197–1209.

RGIK 2022. *Towards standard guidelines for inventorying rock glaciers: baseline concepts (version 4.2.2)*. Fribourg, Switzerland: IPA Action Group Rock glacier inventories and kinematics, 13 p.

Riley, S.J., DeGloria, S.D., and Elliot, R. 1999. 'A terrain ruggedness Index that quantifies topographic heterogeneity', *Intermountain Journal of Sciences* 5, pp. 23–27.

Sass, O. 2006. 'Determination of the internal structure of alpine talus deposits using different geophysical methods (Lechtaler Alps, Austria)', *Geomorphology* 80(1–2), pp. 45–58.

Sattler, K., Anderson, B., Mackintosh, A., Norton, K., and de Róiste, M. 2016. 'Estimating Permafrost Distribution in the Maritime Southern Alps, New Zealand, Based on Climatic Conditions at Rock Glacier Sites', *Frontiers in Earth Science* 4, pp. 166–178.

Scapozza, C., Baron, L., and Lambiel, C. 2015. 'Borehole Logging in Alpine Periglacial Talus Slopes (Valais, Swiss Alps)', *Permafrost and Periglacial Processes* 26(1), pp. 67–83.

Schaffer, N., MacDonell, S., Réveillet, M., Yáñez, E., and Valois, R. 2019. 'Rock glaciers as a water resource in a changing climate in the semiarid Chilean Andes', *Regional Environmental Change* 19(5), pp. 1263–1279.

Schoch, A., Blöthe, J.H., Hoffmann, T., and Schrott, L. 2018. 'Multivariate geostatistical modeling of the spatial sediment distribution in a large scale drainage basin, Upper Rhone, Switzerland', *Geomorphology* 303, pp. 375–392.

Schrott, L. 1994. *Die Solarstrahlung als steuernder Faktor im Geosystem der subtropischen semiariden Hochanden (Agua Negra, San Juan, Argentinien)*. Heidelberg, GER: Selbstverlag des Geographischen Institutes der Universität Heidelberg, 199 p.

Schrott, L. 1996. 'Some geomorphological-hydrological aspects of rock glaciers in the Andes (San Juan, Argentina)', *Zeitschrift für Geomorphologie. Supplementband* 104, pp. 161–173.

Servicio Geológico Minero Argentino (SEGEMAR) 2019. *Cartas Geológicas a escala 1:250.000*. https://sigam.segemar.gov.ar/visor/index.html?mapa=12 (Accessed: 14 June 2023).

Trombotto, D. 1991. 'Untersuchungen zum periglazialen Formenschatz und zu periglazialen Sedimenten in der" Lagunita del Plata", Mendoza, Argentinien', *Heidelberger Geographische Arbeiten* 90, p. 171.

Trombotto, D. 2000. 'Survey of cryogenic processes, periglacial forms and permafrost conditions in South America', *Instituto Geológico; Revista Do Instituto Geologico* 21(1–2), pp. 33–55.

Trombotto Liaudat, D., Wainstein, P.A., and Arenson, L.U. 2014. *Guía Terminológica de la Geocriología Sudamericana. Terminological Guide of the South American Geocryology*. Buenos Aires, ARG: Vazquez Mazzini Editores.

Veitinger, J., Purves, R.S., and Sovilla, B. 2016. 'Potential slab avalanche release area identification from estimated winter terrain: a multi-scale, fuzzy logic approach', *Natural Hazards and Earth System Sciences* 16(10), pp. 2211–2225.

Villarroel, C., Tamburini Beliveau, G., Forte, A., Monserrat, O., and Morvillo, M. 2018. 'DInSAR for a Regional Inventory of Active Rock Glaciers in the Dry Andes Mountains of Argentina and Chile with Sentinel-1 Data', *Remote Sensing* 10(10), p. 1588.

Weiss, A. 2001. *Topographic position and landforms analysis*. San Diego, California, United States: ESRI user conference, Poster Presentation.